

# Automatic Classification of Plutonic Rocks with Machine Learning Applied to Extracted Shades and Colors on iOS Devices

No Author Given

No Institute Given

**Abstract.** Lightness and color are properties used for the classification of plutonic rocks but are difficult to describe because they depend on the experience of the observer. Moreover, the classification of plutonic rocks using various instrumental techniques tend to be expensive and time-consuming. To face this situation, we extracted dominant shades and colors from 283 plutonic rock images in RGB and CIELAB formats to train several machine learning models. The best model was deployed on an iOS application that classifies four classes of plutonic rocks from darkest to lightest: gabbro, diorite, granodiorite, and granite. The best results were for the K-Nearest Neighbors model using CIELAB dominant colors data with accuracy, precision, recall, and F-score of 93%.

**Keywords:** Plutonic Rock Classification, Feature Extraction, Dominant Colors, Machine Learning, iOS Application

## 1 Introduction

Plutonic rocks are formed when magma cools and solidifies below the Earth's surface. Lightness and color are properties used for the classification of these rocks. Color changes in rocks may indicate changes in other rock properties (mineral assemblage, texture, organic carbon content, and more), that is why color is a key property for rock classification. However, these attributes are difficult to describe because perceived shades and colors in rocks depend on the experience of the observer [1]. Moreover, the instruments for accurate rock classification are time-consuming and expensive making it prohibitive for geology students and amateurs.

Our contribution in this research work is to extract dominant shades and colors from plutonic rock images to train several machine learning algorithms and deploy the best model on an iOS application for the automatic classification of four classes of plutonic rocks: gabbro, diorite, granodiorite, and granite. No such application exists. A mobile application offers the flexibility to carry out the classification in real time and could be an alternative to expensive traditional methods of rock classification.

Specifically, our three objectives are as follows:

- Determine the best  $k$  number of clusters to use in the K-means algorithm to extract the dominant colors in terms of RGB and CIELAB color spaces from 283 images of plutonic rocks.
- Use the extracted dominant colors and their percentage of pixels in the images to train the following machine learning algorithms: Logistic Regression (LR), K-Nearest Neighbors (KNN), Decision Trees (DT), Support Vector Machines (SVM), and a Convolutional Neural Network (CNN).
- Validate the generated models and deploy the best model in an iOS mobile application.

This article is organized as follows: Section 2 introduces the underpinnings of our approach. Section 3 presents the state-of-the-art of mineral and rock classification with machine learning. Section 4 describes the methodology. Section 5 presents and discusses the results. Finally, Section 6 presents the conclusions and future work.

## 2 Underpinnings of our Approach

Our approach is based on the following concepts (see Fig. 1).

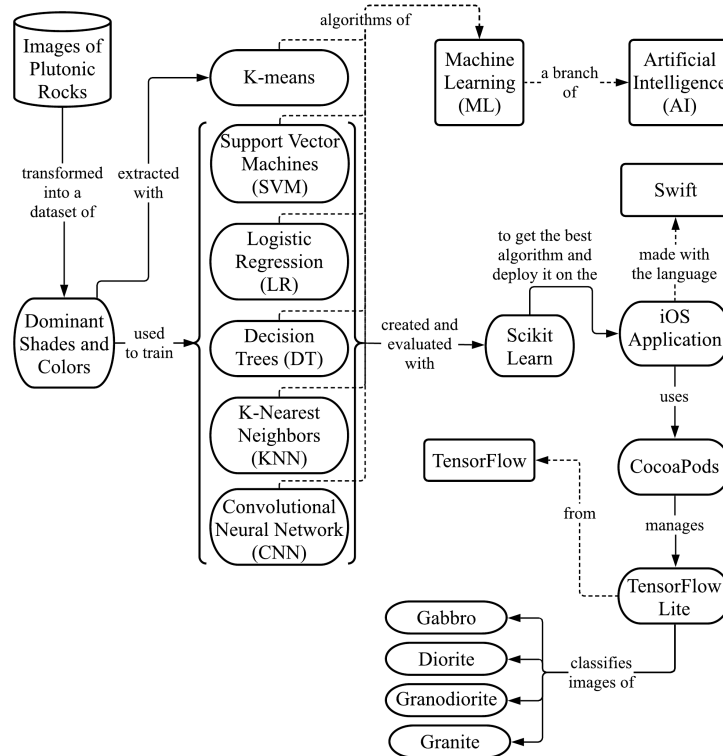


**Fig. 1.** Underpinnings of our approach

## 2.1 Plutonic rocks

Plutonic rocks crystalize inside the Earth's crust from magma are generally coarse-grained and compositionally classified by the proportion of minerals in it. According to [2]:

- Gabbro is a plutonic rock composed mainly of calcium plagioclase and pyroxene, with or without olivine or amphibole. It is the intrusive equivalent of basalt and is distinguished from diorite by the nature of plagioclase, which is higher in calcium than in sodium.
- Diorite has about the same structural properties as granite but darker color and more limited occurrence. Commonly it is composed of about two-thirds plagioclase feldspar and one-third dark-coloured minerals, such as hornblende or biotite. The presence of more sodium-rich plagioclase and less calcium-rich plagioclase is the main distinction between diorite and gabbro [3].
- Granodiorite is characterized by quartz with plagioclase constituting more than 2/3 of the total feldspars. Generally, together with granite, it is the most abundant rock of the great batholiths. Its volcanic equivalent is dacite. Granodiorite is similar to granite, but with less potassium feldspar and more plagioclase, hornblende, and biotite.
- Granite is a light-colored rock characterized by coarse to medium crystal size, composed of approximately equal amounts of quartz, potassium feldspar, and plagioclase as essential minerals, and smaller amounts of other minerals, such as biotite, muscovite or hornblende.

## 2.2 Machine Learning

Machine learning is a branch of artificial intelligence that lies at the intersection between computer science, engineering and statistics, and often appears in other disciplines. Machine learning systems can be classified according to the type of supervision they get during training [4, 5]. In this way, there are two major categories:

**Supervised learning.** In supervised learning, a typical task is classification. The training set fed to the algorithm includes the desired solutions, called labels [5]. Some common supervised learning algorithms are described as follows:

- Logistic Regression (LR) is commonly used to estimate the probability that an instance belongs to a particular class. LR computes a weighted sum of the input features (plus a bias term) and outputs the logistic of this result. The logistic is a sigmoid function that outputs a number between 0 and 1. This makes LR a binary classifier [5].
- K-Nearest Neighbors (KNN) is used to predict the label of a new point finding a predefined number of training samples closest in distance to that point. Being a non-parametric method, it is often successful in classifications where the decision boundary is very irregular [6].

- Decision Trees (DT) algorithm consists of split nodes and leaf nodes. Each split node performs a split decision and routes a data sample either to the left or the right child node. Leaves represent the labels, non-leaf nodes are the input features, and branches represent conjunctions of features that lead to the classifications [7, 8].
- Support Vector Machines (SVM) is a powerful and versatile algorithm, particularly well suited for classification of complex small- or medium-sized datasets. The data is plotted in a n-dimensional space (number of features) and a decision boundary (hyperplane) splits that space into classes [4, 5].
- Convolutional Neural Networks (CNNs) emerged from the study of the brain’s visual cortex. The CNN’s architecture consists of several connected layers allowing the network to concentrate on small low-level features in the first hidden layer to assemble them into larger higher-level features in the next layers. Their most important building block is the convolutional layer [5].

**Unsupervised learning.** In unsupervised learning the training data is unlabeled. K-means is one of the most important unsupervised learning algorithms. K-means can cluster unlabeled data very quickly and efficiently, often in a few iterations. Its goal is to group similar instances together into a  $k$  number of clusters assigning each instance to one of the clusters [5].

### 2.3 Dominant colors

The dominant colors refer to the principal colors presented in an image. These colors are selected grouping the image pixels according to their color in the color space (RGB or CIELAB). The colors are represented as a three-value vector. The average color of each group is a dominant color and its percentage is the number of pixels in that group.

On one hand, in RGB (Red, Green, Blue) the light spectra of varying fractions of the three primary color channels combine to make new colors. Each channel has intensity values from 0 to 1 scaled by the number of bits used to represent it. The 24-bit color cube used in this research work scales the channel values in the range of 0–255.

On the other hand, CIELAB has the property of being perceptually uniform (useful to measure the similarity between two colors) and is designed to approximate human vision. The  $L$  channel represents the brightness of each pixel varying between 0 and 100. The  $a$  (red/green) and  $b$  (yellow/blue) channels correspond to the chromaticity components and contain information about the color of a pixel, independent of its brightness. Their values vary between -127 and 127.

### 2.4 Underlying technologies

**Scikit-learn.** Scikit-learn<sup>1</sup> is a Python module that integrates a wide range of state-of-the-art machine learning algorithms for medium-scale supervised and

---

<sup>1</sup><https://www.scikit-learn.org>

unsupervised problems. This library focuses on bringing machine learning to non-specialists using a general-purpose high-level language. Emphasis is put on ease of use, performance, documentation, and API consistency. It has minimal dependencies and is distributed under the simplified Berkeley Source Distribution (BSD) license, encouraging its use in both academic and commercial settings [9].

**Tensorflow.** TensorFlow<sup>2</sup> is an interface for expressing machine learning algorithms and an implementation for executing such algorithms. A computation expressed using TensorFlow can be executed with little or no change on a wide variety of heterogeneous systems, ranging from mobile devices such as phones and tablets up to large-scale distributed systems with hundreds of machines and thousands of computational devices such as GPUs [10].

**Tensorflow Lite.** TensorFlow Lite<sup>3</sup> is a set of tools to help developers run TensorFlow machine learning models on mobile, embedded, and Internet of Things (IoT) devices [11]. TensorFlow Lite consists of two main components:

- The interpreter, which runs specially optimized models on many different hardware types.
- The converter, which converts TensorFlow models into an efficient form for use by the interpreter, and can introduce optimizations to improve them.

**Swift.** Swift<sup>4</sup> is an open source programming language designed by Apple for Apple platforms and is better in type safety, security, and hardware performance than Objective-C. Community members actively work to port it even to more platforms like Linux [12].

**CocoaPods.** CocoaPods<sup>5</sup> is a dependency manager for Swift and Objective-C Cocoa projects. It resolves dependencies between libraries, fetches the resulting source code, then links it together in an Xcode workspace to build a single project [13].

### 3 Related Work

Over the last decade, there has been considerable progress in the application of machine learning to geochemistry [14]. In this section we present relevant research work in three areas: image classification of rock lithology using machine learning, rock classification with machine learning on mobile devices, and recognition of mineral images applying machine learning and feature extraction. Table 1 summarizes the works presented in this section.

---

<sup>2</sup><https://www.tensorflow.org>

<sup>3</sup><https://www.tensorflow.org/lite>

<sup>4</sup><https://swift.org>

<sup>5</sup><https://cocoapods.org>

**Table 1.** Comparison table of the articles described in the related work

Author Year	Dataset	Algorithm of extraction	Extracted features	Training dataset	Best model	Results
Fan et al. [15] 2020	3,208 images of 28 rock lithology categories	-	-	80% of the images	SqueezeNet	Accuracy: 94.55% File size: 9.2 MB Execution time: 736-366 ms
Fan et al. [16] 2020	3,795 images of 30 different rock types	-	-	80% of the images	ShuffleNet	Accuracy: 95.30% File size: 18.2 MB Execution time: 786 ms
Ran et al. [17] 2019	14,589 patches from 2,290 images of 6 rock types (granite, limestone, conglomerate, sandstone, shale, mylonite)	-	-	60% of the patches	3-layer CNN	Accuracy: 97.76%
Zhang et al. [18] 2019	481 images of 4 minerals (K-feldspar, perthite, plagioclase, and quartz)	Inception v3 CNN	High-level features like chromatic aberration and texture	90% of extracted features	Stacking model (LR, SVM, and MLP)	Accuracy: 90.9%
Maitre et al. [19] 2019	3,192 sub-images of the views taken at different angles to a surface with 27 mineral grain species	SLIC algorithm	Color and Peak intensity of superpixel histograms	70% of extracted features	Random Forest (RF)	Accuracy: 89%
Cheng and Guo [20] 2017	4,200 images of 3 feldspar sandstone rock types (coarse, medium granular, and fine)	-	-	75% of the images	6-layer CNN	Accuracy: 98.5%

### 3.1 Image classification of rock lithology using machine learning

In [17], Ran et al. proposed a CNN model for the classification of six rock types (granite, limestone, conglomerate, sandstone, shale, mylonite) and compared their results with four other common machine learning models. A total of 2,290 images were labeled according to the clarity of the rock and cropped into 14,589 sample patches of  $512 \times 512$  pixels compressed to  $128 \times 128$  pixels. 60% of the patches of each rock type were selected for the training dataset, 20% for the validation dataset, and 20% for the testing dataset. Their proposed CNN model achieved the highest overall accuracy of 97.76% compared with the other models: SVM, AlexNet, GoogleLeNet Inception v3, and VGGNet-16.

In [20], Cheng and Guo proposed a deep CNN to identify the granularity of feldspar sandstone rocks in images under three color spaces: RGB, YCbCr, and HSV. A total of 4,200 images were collected from rocks of an oil field in Ordos and divided into three types of granularity: coarse, medium granular, and fine. The RGB images were normalized to  $224 \times 224$  pixels and converted to YCbCr and HSV. The proposed CNN was a 6-layer structure of 4 convoluted layers with ReLU as the activation function and 2 fully connected layers with Softmax as the classifier. The model was trained for each color space with 75% of the experimental data, a batch size of 100, and different kernel sizes and learning rates. The lowest error rates were obtained with the learning rate of 0.0005, the kernel sizes of 11, 5, 3, and 3 for each convolutional layer respectively, and the cross-validation for HSV color space. In RGB color space, the classification accuracy achieved 98.5%.

### 3.2 Rock classification with machine learning on mobile devices

In [15], Fan et al. created a method for rock lithology recognition on Android devices based on the two lightweight SqueezeNet and MobileNet CNNs. These models were compared with ResNet50, a heavyweight model. The images were selected from the China Geological Survey dataset that contains images of 28 rock categories taken by a smartphone camera. The 3,208 images were reduced to  $214 \times 214$  pixels and the 80% of those images was used to train the two CNNs pretrained with the ImageNet dataset. The achieved occupation sizes were 19.6, 36.8, and 232.7 MB for MobileNet, SqueezeNet, and ResNet50. SqueezeNet was almost two times faster than MobileNet and 7 times faster than ResNet50. A rock recognition software based on the trained models was developed for Android devices. The results for SqueezeNet and MobileNet on Android smartphones were: execution time from 736 to 366 and 1,218 to 523 milliseconds, and recognition accuracies of 94.55% and 93.27%.

Also in [16], Fan et al. improved their work using a model based on ShuffleNet for quick and accurate rock lithology recognition with smartphones and compared it with their previous work of MobileNet and SqueezeNet. They selected 3,795 images of 30 different kinds of rocks collected from multiple locations in East China. The ShuffleNet model was trained using 80% of the dataset, 3,600 iteration steps, a learning rate of 0.008, and the parameters imported by

the transfer learning method using the ImageNet dataset. ShuffleNet occupied a space of 18.2 MB compared to MobileNet, SqueezeNet, and ResNet50 that occupied 34.5, 25, and 219.4 MB respectively. An Android application was created using each model. The average recognition time for a single rock in ShuffleNet was 786 milliseconds. It reached an accuracy of 97.65% on a PC.

### **3.3 Recognition of mineral images applying machine learning and feature extraction**

In [18], Zhang et al. worked on the intelligent identification of rock-mineral images using ensemble machine learning algorithms (model stacking). A total of 481 images of four minerals (K-feldspar, perthite, plagioclase, and quartz) were obtained with a camera on top of a microscope. The target RGB images were cropped to cover the minerals and then processed to have  $299 \times 299$  pixels. A deep learning model based on Inception-v3 was adopted to extract high-level features (such as chromatic aberration and texture) from the images and train the algorithms of LR, SVM, KNN, Random Forest (RF), Multilayer Perceptron (MLP), and Gaussian Naive Bayes (GNB). LR, SVM, and MLP had a significant effect on extracted features, with higher accuracy (90.0%, 90.6%, and 89.8%) than the other models. The new features generated by these three models were employed for the model stacking in a new instance of LR. The stacking model showed a better performance than the single models, with an accuracy of 90.9%.

In [19], Maitre et al. created several models of supervised machine learning to recognize mineral grains in a sample surface containing grains of 27 different mineral species (plagioclase, augite, background, hypersthene, ilmenite, magnetite, titanite, hornblende, etc.). The surface was scanned with an automated Scanning Electron Microscopy (SEM). Several views of the same surface were taken with a stereo-zoom binocular microscope to construct a large mosaic RGB image. Both images were divided into 3,192 sub-images of  $600 \times 600$  pixels. To label the grains of the mosaic image, the simple linear iterative clustering (SLIC) algorithm was applied for superpixel segmentation to match each superpixel of the mosaic's sub-images with the superpixels of the SEM's scan sub-images. From the computed RGB superpixel histograms, the color intensity (quantile) and peak intensity (ratio between the number of pixels in the first and second maximum bins to total number of pixels) were extracted as features for each superpixels. KNN, RF, and Classification and Regression Trees (CART) algorithms were trained with 70% of the extracted features, and tested with the other 30% using the kappa statistics, precision, recall, and F-score indicators. The RF algorithm gave the best results with a global accuracy of 89%.

### **3.4 Discussion**

Machine learning has been an effective way for image classification in geochemistry. Specifically, feature reduction was applied in [18, 19] using deep learning and the simple linear iterative clustering (SLIC) algorithm to extract high-level

features from images of mineral samples before training the machine learning models. Although these works showed good results in the classification of mineral samples, the number of extracted features was very large.

Four articles [15, 16, 17, 20] introduce CNN topologies and analyze the performance of the models generated for rock lithology classification using all the image features rather than extracted features. The evaluation of the models showed good results. Also, the models in the research works were trained with diverse types of rocks instead of using only plutonic rocks. Finally, in [15, 16] the created models were deployed on an Android mobile application for the classification of rocks. However, there are no works presenting the deployment of machine learning for the classification of plutonic rocks on iOS devices.

## 4 Methodology

This section describes the steps followed in this research work.

### 4.1 Getting the images of the plutonic rocks

The images of plutonic rocks were provided by the Department of Earth and Biological Sciences at Loma Linda University. We use pictures from plutonic rocks that were classified by using petrography and chemistry data. Specifically, the dataset contains 283 image patches selected from the 81 original images of four classes of plutonic rocks: gabbro, diorite, granodiorite, and granite. In the experiments we used clean rock samples with negligible weathering or alteration visible to the naked eye. The images used in the following experiments were organized in subfolders according to their class and are available online<sup>6</sup>. Table 2 shows the number of images per class.

**Table 2.** Number of images per class

Class	Number of images
Diorite	78
Gabbro	65
Granite	70
Granodiorite	70
<b>Total of images</b>	<b>283</b>

### 4.2 Preparing the data

In this step, the images were processed in order to obtain the color values of the image pixels in RGB and CIELAB color spaces.

First, all files in the subfolders were processed in RGB format and labeled according to their container subfolder (e.g. images in the granite subfolder are

---

<sup>6</sup><https://bit.ly/2P9JLEc>

labeled as granite). Afterwards, the RGB values of the image pixels were converted to CIELAB values using the “rgb2lab” function of the “color” class of the Scikit-image module. In this way, it is possible to train the models in the two color spaces and determine which color format is the most appropriate for classifying the dominant colors of the 4 classes of plutonic rocks. The notebook with the source code for data preparation is available online<sup>7</sup>.

#### 4.3 Determining the best number of color clusters

The K-means algorithm was used to extract the dominant colors from the images. The Elbow method was used to calculate the optimal number of clusters  $k$  to use by the K-means algorithm. This method consists of iterating in a range of possible cluster numbers and determine the best one. The  $k$  value ranged from 2 to 20 was declared to obtain the scores of K-means at each cluster number. Finally, we plotted the scores with their respective  $k$  number. The number at the elbow in the plot indicates the best  $k$  number of clusters, which is 4 for this experiment (see Fig. 2).

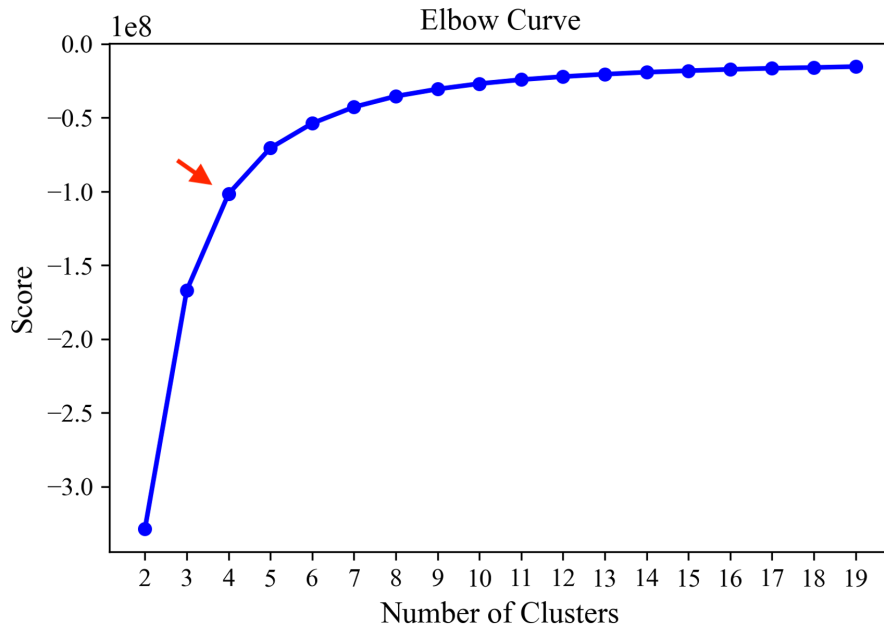


**Fig. 2.** The Elbow method returned the optimal  $k$  number of clusters

---

<sup>7</sup><http://bit.ly/3pyh3JL>

#### 4.4 Color extraction

In this step, the dominant colors were extracted from the rock images. In Listing 1.1, the “get\_dominant\_colors” function receives the pixel values of an image to train the K-means algorithm with  $k$  clusters. In line 6, K-means works by separating the pixels of the image into 4 clusters of similarly colored pixels. The colors at each cluster center reflect the average value of the attributes of all members of a cluster. The percentage of a cluster is the number of pixels within that color cluster and is calculated in lines 8 to 10. Finally, the centroid of each cluster and its percentage are sorted in increasing order of percentage and added to a features list in lines 12 to 17. The returned list in line 19 are the sixteen features: the four dominant colors represented by the three channels of the selected color format and the percentage of each dominant color (see Fig. 3).

```

1 from sklearn.cluster import KMeans
2 CLUSTERS = 4
3
4 def get_dominant_colors(img):
5     reshape = img.reshape((img.shape[0] * img.shape[1], img.shape[2]))
6     cluster = KMeans(n_clusters=CLUSTERS).fit(reshape)
7
8     lb = np.arange(0, len(np.unique(cluster.labels_))+1)
9     (hist, _) = np.histogram(cluster.labels_, bins=lb)
10    hist = hist.astype("float"); hist /= hist.sum()
11
12    features = []
13    colors = sorted([(percent,color) for (percent,color) in
14        zip(hist,cluster.cluster_centers_)])
15    for (percent, color) in colors:
16        features.extend(color)
17        features.append(percent)
18    return features

```

**Listing 1.1.** Function to extract the dominant colors from a single image

In Listing 1.2, the processed data in RGB format is iterated in lines 4 to 6 and the dominant colors are extracted in line 5 with the function described in Listing 1.1. The colors are added to a new list of extracted colors in line 6. This process is also made for the CIELAB data in lines 8 and 9. Finally, the extracted colors in RGB and CIELAB formats are saved together with their respective rock label in different CSV files. These files were used in the next step to train the machine learning algorithms. The CSV files with the extracted dominant colors in RGB and CIELAB color spaces are available online<sup>8,9</sup>.

```

1 extracted_rgb = []; extracted_lab = []
2
3 for rgb, lab in zip(x_rgb, x_lab):
4     features = get_dominant_colors(rgb)
5     extracted_rgb.append(features)
6     features = get_dominant_colors(lab)
7     extracted_lab.append(features)

```

**Listing 1.2.** Iterate original data to extract dominant colors

---

<sup>8</sup>[https://github.com/sarah-hs/Color-extraction/blob/main/colors\\_RGB.csv](https://github.com/sarah-hs/Color-extraction/blob/main/colors_RGB.csv)

<sup>9</sup>[https://github.com/sarah-hs/Color-extraction/blob/main/colors\\_LAB.csv](https://github.com/sarah-hs/Color-extraction/blob/main/colors_LAB.csv)

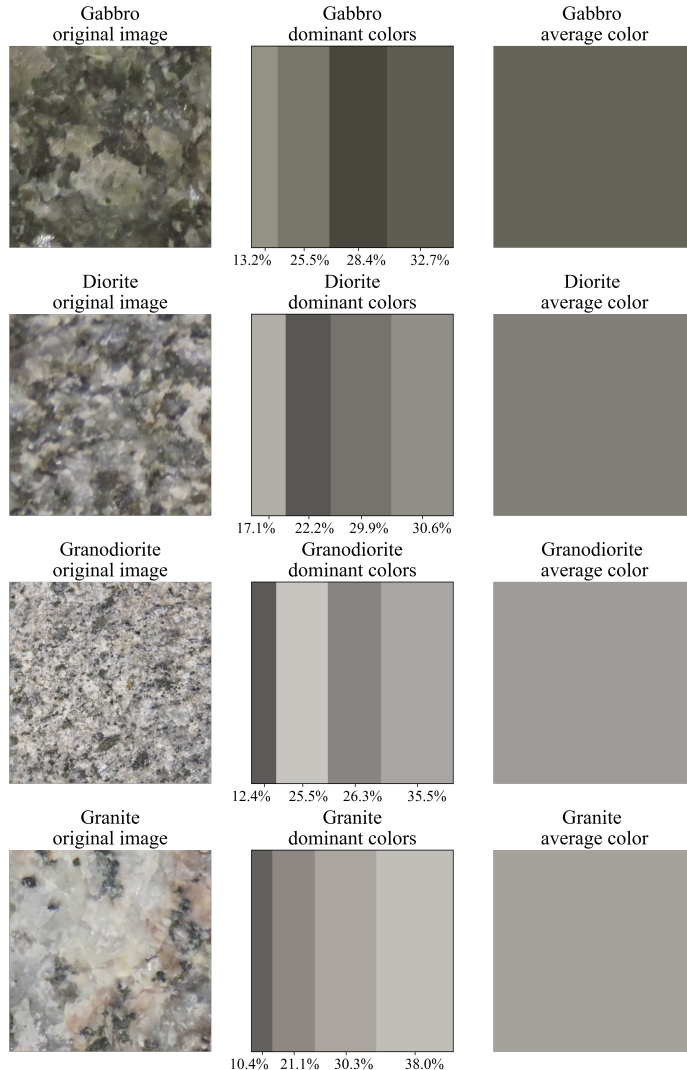


**Fig. 3.** Sample rocks with their dominant colors in percentage order and their average color

#### 4.5 Data normalization and label encoding

First, in this step we loaded the dominant colors data from the CSV files generated in the previous step. The dominant colors data are the features loaded into  $x$ , and the rock classes are the labels loaded into  $y$ . Second, in order to train and test the models, the  $x$  and  $y$  data were divided into a training set of 80% and a test set of 20% using the “train\_test\_split” function of the “model\_selection” class of Scikit-learn. Afterwards, we normalized the  $x$  data of train and test

sets using the “MinMaxScaler” function of the “preprocessing” class of Scikit-learn. This function scales each feature to a given range of 0 to 1. Finally, we encoded the  $y$  data in order to train the machine learning models transforming the labels into values from 0 to 3 representing the four rock classes of plutonic rocks: gabbro, diorite, granodiorite, and granite respectively. The encoding process was made with the “LabelEncoder” function of the “preprocessing” class of Scikit-learn.

#### 4.6 Training the different algorithms with the extracted dominant colors

The following five machine learning models were trained in this experiment using the RGB and afterwards the CIELAB dominant colors data: LR, KNN, DT, SVM, and a sequential CNN topology with the following layers: a convolutional layer (32 filters, kernel size = 2, padding = same, input shape = 16 x 1, and activation = RELU); a max pooling layer (pool size = 2); a convolutional layer (64 filters, kernel size = 2, padding = same, and activation = RELU); a max pooling layer (pool size = 2); a flatten layer; and two dense layers, one with 64 filters and RELU activation and another one with 4 filters, one per class, and a SOFTMAX activation function. The notebooks showing the code for training and validation of the generated models with RGB and CIELAB data are available online<sup>10,11</sup>.

#### 4.7 Creation of the iOS application

The best model was exported with Tensorflow Lite and deployed in an iOS mobile application to make the classification of images of four classes of plutonic rocks in real time.

The main requirements to develop the application were the Xcode IDE, the Xcode command-line tools, a valid Apple Developer ID, and the CocoaPods dependency manager. The application was written mostly in Swift and uses the following two libraries to perform the extraction of the dominant colors and the rock image classification:

- The DominantColor<sup>12</sup> dependency is an open source library written in Swift. It finds the dominant colors of an image using the K-means clustering algorithm.
- The TensorFlowLite Swift<sup>13</sup> library is TensorFlow’s lightweight solution for Swift developers. It enables low-latency inference of on-device machine learning models with a small binary size and fast performance supporting hardware acceleration. For the application, TensorFlowLiteSwift pod name was added into the project’s Podfile, and from command line the library was resolved into the Xcode project by the CocoaPods dependency manager.

---

<sup>10</sup><https://github.com/sarah-hs/Color-extraction/blob/main/train-RGB.ipynb>

<sup>11</sup><https://github.com/sarah-hs/Color-extraction/blob/main/train-LAB.ipynb>

<sup>12</sup><https://github.com/indragiek/DominantColor>

<sup>13</sup><https://github.com/tensorflow/tensorflow/tree/master/tensorflow/lite/swift>

## 5 Results

### 5.1 Results

Table 3 shows the average accuracy, precision, recall, and F-score results of each model evaluated with the test sets of dominant colors in RGB and CIELAB color formats. The models generated with the KNN, SVM, LR, and CNN algorithms gave better results with CIELAB data than with RGB data. The results with the DT model were better in RGB. The best results were for the KNN model using the CIELAB dominant colors data with an accuracy, precision, recall, and F-score of 93%. The training time of the KNN model was 4.33 minutes.

**Table 3.** Results of the models in terms of accuracy, precision, recall, and F-score

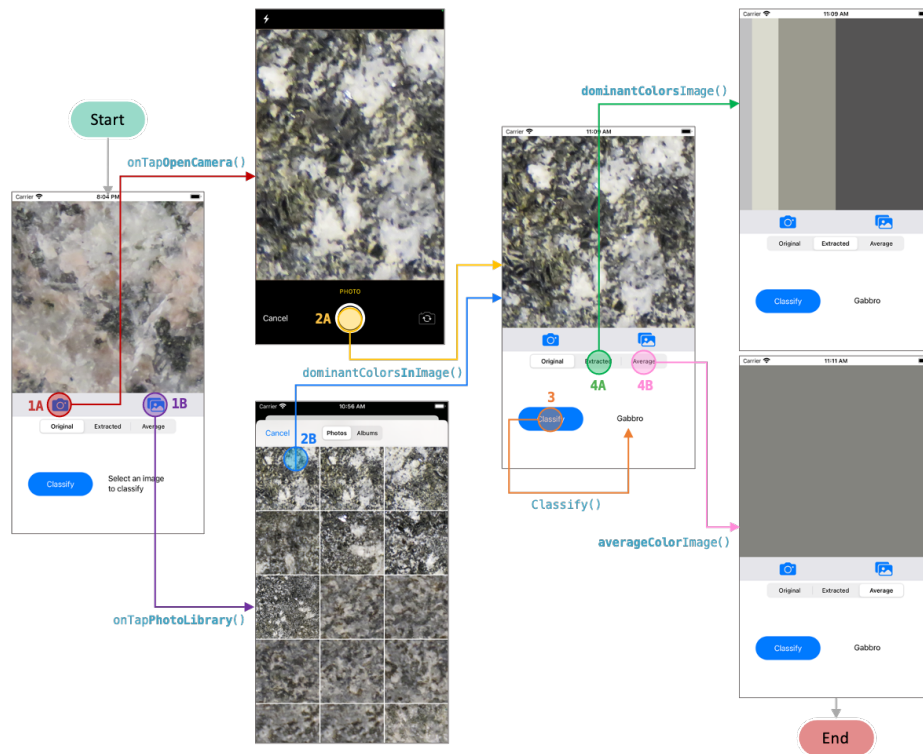
Model	Accuracy	Precision	Recall	F-score
with CIELAB dominant colors				
CNN	0.82	0.82	0.83	0.82
DT	0.72	0.72	0.72	0.72
KNN	0.93	0.93	0.93	0.93
LR	0.63	0.64	0.66	0.63
SVM	0.80	0.82	0.82	0.80
with RGB dominant colors				
CNN	0.68	0.68	0.70	0.68
DT	0.73	0.75	0.74	0.74
KNN	0.79	0.80	0.79	0.79
LR	0.63	0.64	0.65	0.62
SVM	0.52	0.60	0.49	0.46

Table 4 shows the evaluation results of the KNN model for each rock class in terms of precision, recall, and F-score using the CIELAB dominant colors data.

**Table 4.** Results of KNN for each rock class with CIELAB data

Class	Precision	Recall	F-score
Gabbro	0.93	1.00	0.96
Diorite	0.89	1.00	0.94
Granodiorite	0.92	0.79	0.85
Granite	1.00	0.92	0.96

The KNN model was deployed on the iOS application (see Fig. 4). There are two ways to make the classification of new rocks on this application. The first way is taking a picture with the “Open Camera” button shown in step 1A of Fig. 4. When camera opens, the new scene of step 2A appears and displays the device camera. The second way is choosing a photo from the “Photo Library”. The “Open Library” button in step 1B opens the photo library of the device as shown in step 2B. The extraction of the dominant colors is performed after the image was loaded with the “dominantColorsInImage” function. Thereafter, the “Classify” button in step 3 is enabled to classify the new rock image into: gabbro, diorite, granodiorite, or granite. When the button is pressed the extracted colors are converted to CIELAB and sorted in ascending order by their percentage of pixels in the image. These colors and their percentage are used as the input tensor for the model imported from the “tflite” file containing its graph. Optionally, the dominant colors and the average colors of the selected image can be displayed pressing the “Extracted” and “Average” buttons of steps 4A and 4B respectively.



**Fig. 4.** Application workflow

At runtime, the classification with the KNN exported model took 339.87 milliseconds. The size of the model was 0.018 MB.

## 6 Conclusions and future work

In this research work, five machine learning algorithms were trained with just the four dominant colors extracted from images of plutonic rocks. The best model was found with the KNN algorithm trained with the dominant colors in the CIELAB color format of 283 images. The KNN model has an accuracy, precision, recall, and F-score values of 93%.

As future work, the datasets for training and validation will be extended with a larger number of plutonic rock images taken in the field, rather than in the lab. Also, images will be taken under different conditions – different distances, angles, and lighting effects, e.g., blue vs. cloudy sky, with weathering or alteration, shadows, vegetation, and moss.

## References

- [1] Natural Resources Conservation Service, “Part 631: Geology,” in *National Engineering Handbook*, 210-VI, 2012, ch. 4, p. 7. [Online]. Available: <https://directives.sc.egov.usda.gov/OpenNonWebContent.aspx?content=31848.wba>.
- [2] J. Vera, B. Alonso, E. Ancochea, R. Capote, E. Custodio, M. Gutiérrez, A. Pérez, A. Sahuquillo, X. Solans, F. Vázquez, C. Zazo, F. Bastida, F. Bea, F. Fernández, J. Galindo, A. García, F. González, P. González, M. J. Huertas, J. R. Martínez, J. M. Molina, J. Morales, M. Prieto, F. Velasco, P. Martínez, and P. Cuesta, *RACEFEN Glosario de geología*, Spanish, España: Real academia de ciencias exactas, físicas y naturales. [Online]. Available: [http://www.ugr.es/~agcasco/personal/rac\\_geologia/0\\_rac.htm](http://www.ugr.es/~agcasco/personal/rac_geologia/0_rac.htm).
- [3] Encyclopædia Britannica, *Diorite*, English, Encyclopædia Britannica, Jan. 2009. [Online]. Available: <https://www.britannica.com/science/diorite>.
- [4] P. Harrington, *Machine Learning in Action*. MANNING PUBN, Apr. 1, 2012, 384 pp., ISBN: 1617290181. [Online]. Available: <https://www.manning.com/books/machine-learning-in-action>.
- [5] A. Géron, *Hands-on Machine Learning with Scikit-Learn, Keras, and TensorFlow*. O'Reilly UK Ltd., Oct. 1, 2019, 819 pp., ISBN: 1492032646.
- [6] Scikit-learn, *Nearest Neighbors*, English, Scikit-learn. [Online]. Available: <https://scikit-learn.org/stable/modules/neighbors.html#id5>.

- [7] C. Reinders, H. Ackermann, M. Y. Yang, and B. Rosenthal, “Chapter 4 - Learning Convolutional Neural Networks for Object Detection with Very Little Training Data,” in *Multimodal Scene Understanding*, M. Y. Yang, B. Rosenthal, and V. Murino, Eds., Academic Press, 2019, pp. 65–100, ISBN: 978-0-12-817358-9. DOI: <https://doi.org/10.1016/B978-0-12-817358-9.00010-X>.
- [8] L. Tan, “Chapter 17 - Code Comment Analysis for Improving Software Quality,” in *The Art and Science of Analyzing Software Data*, C. Bird, T. Menzies, and T. Zimmermann, Eds., Boston: Morgan Kaufmann, 2015, pp. 493–517, ISBN: 978-0-12-411519-4. DOI: <https://doi.org/10.1016/B978-0-12-411519-4.00017-3>.
- [9] F. Pedregosa, G. Varoquaux, A. Gramfort, V. Michel, B. Thirion, O. Grisel, M. Blondel, P. Prettenhofer, R. Weiss, V. Dubourg, J. Vanderplas, A. Passos, D. Cournapeau, M. Brucher, M. Perrot, and E. Duchesnay, “Scikit-learn: Machine Learning in Python,” *Journal of Machine Learning Research*, vol. 12, no. 85, pp. 2825–2830, 2011. [Online]. Available: <http://jmlr.org/papers/v12/pedregosa11a.html>.
- [10] M. Abadi, A. Agarwal, P. Barham, E. Brevdo, Z. Chen, C. Citro, G. S. Corrado, A. Davis, J. Dean, M. Devin, S. Ghemawat, I. Goodfellow, A. Harp, G. Irving, M. Isard, Y. Jia, R. Jozefowicz, L. Kaiser, M. Kudlur, J. Levenberg, D. Mane, R. Monga, S. Moore, D. Murray, C. Olah, M. Schuster, J. Shlens, B. Steiner, I. Sutskever, K. Talwar, P. Tucker, V. Vanhoucke, V. Vasudevan, F. Viegas, O. Vinyals, P. Warden, M. Wattenberg, M. Wicke, Y. Yu, and X. Zheng, “TensorFlow: Large-Scale Machine Learning on Heterogeneous Distributed Systems,” Mar. 14, 2016. arXiv: 1603.04467 [cs.DC].
- [11] TensorFlow, *TensorFlow Lite guide*, English, comp. software, TensorFlow, Mar. 2020. [Online]. Available: <https://www.tensorflow.org/lite/guide>.
- [12] Apple, *Swift. the powerful programming language that is also easy to learn.* English, Tech. Rep., Apple. [Online]. Available: <https://developer.apple.com/swift/>.
- [13] CocoaPods, *What is CocoaPods*, English, comp. software, CocoaPods. [Online]. Available: <https://guides.cocoapods.org/using/getting-started.html>.
- [14] D. J. Lary, G. K. Zewdie, X. Liu, D. Wu, E. Levetin, R. J. Allee, N. Malakar, A. Walker, H. Mussa, A. Mannino, and D. Aurin, “Machine Learning Applications for Earth Observation,” in *Earth Observation Open Science and Innovation*, C. Mathieu Pierre-Philippe and Aubrecht, Ed., Cham: Springer International Publishing, 2018, pp. 165–218, ISBN: 978-3-319-65633-5. DOI: [https://doi.org/10.1007/978-3-319-65633-5\\_8](https://doi.org/10.1007/978-3-319-65633-5_8).
- [15] G. Fan, F. Chen, D. Chen, and Y. Dong, “Recognizing Multiple Types of Rocks Quickly and Accurately Based on Lightweight CNNs Model,” *IEEE Access*, vol. 8, pp. 55 269–55 278, 2020. DOI: <https://doi.org/10.1109/access.2020.2982017>.

- [16] G. Fan, F. Chen, D. Chen, Y. Li, and Y. Dong, “A Deep Learning Model for Quick and Accurate Rock Recognition with Smartphones,” *Mobile Information Systems*, vol. 2020, pp. 1–14, 2020. DOI: <https://doi.org/10.1155/2020/7462524>.
- [17] X. Ran, L. Xue, Y. Zhang, Z. Liu, X. Sang, and J. He, “Rock Classification from Field Image Patches Analyzed Using a Deep Convolutional Neural Network,” *Mathematics*, vol. 7, no. 8, p. 755, 2019. DOI: <https://doi.org/10.3390/math7080755>.
- [18] Y. Zhang, M. Li, S. Han, Q. Ren, and J. Shi, “Intelligent Identification for Rock-Mineral Microscopic Images Using Ensemble Machine Learning Algorithms,” *Sensors*, vol. 19, no. 18, p. 3914, 2019. DOI: <https://doi.org/10.3390/s19183914>.
- [19] J. Maitre, K. Bouchard, and L. P. Bédard, “Mineral grains recognition using computer vision and machine learning,” *Computers & Geosciences*, vol. 130, pp. 84–93, 2019. DOI: <https://doi.org/10.1016/j.cageo.2019.05.009>.
- [20] G. Cheng and W. Guo, “Rock images classification by using deep convolution neural network,” *Journal of Physics: Conference Series*, vol. 887, p. 012089, 2017. DOI: <https://doi.org/10.1088/1742-6596/887/1/012089>.